Theoretical and experimental study on steel open-web sandwich floor with flanged cruciform section shear key

Ruilin Shen[a,b] (iD)**, Jianchun Xiao[a,b]*** (iD)**, Kejian Ma[a,b]** (iD)**, Jiayi Mao[c]** (iD)**, Guiping Li[d]** (iD)**, Weiyi Zeng[a,b]** (iD)**, Qin Wang[a,b]** (iD)

a Space Structures Research Center, Guizhou University, Guiyang, China. E-mail: 372553672@qq.com, jcxiao@gzu.edu.cn, makejian2002@163.com, 630084497@qq.com, chhwq@qq.com
b Key Laboratory of Structural Engineering of Guizhou Province, Guiyang, China
c Guiyang City People's Air Defense Office, Guiyang, China. E-mail: 475503188@qq.com
d School of Civil Engineering, Guizhou Institute of Technology, Guiyang, China. E-mail: 825949222@qq.com

* Corresponding author
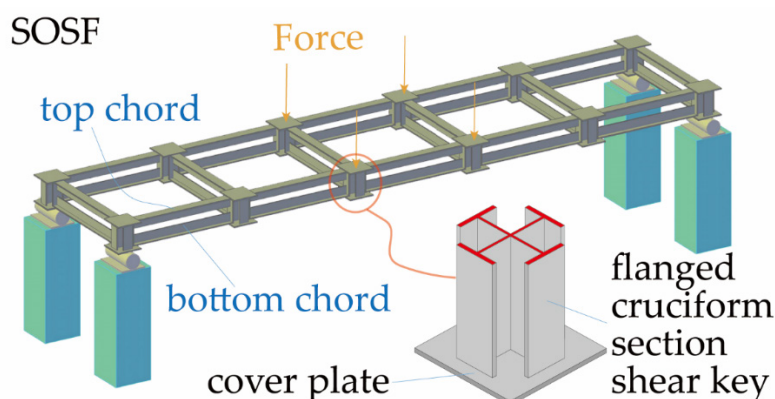
https://doi.org/10.1590/1679-78255897

Abstract

Steel open-web sandwich floors (SOSFs) have been applied in several pioneering industrial and public buildings. The traditional square tube shear key (STSK) is changed into a flanged cruciform section shear key (FCSK) to further improve the bearing capacity of SOSFs. A half-scale test model is designed. A graded static loading test is performed to measure deflection and strain. The calculation formula of the intersection beam analogy method (IBAM) considering the influence of shear stiffness is proposed. A finite element (FE) analysis was also performed. The results of the test, IBAM and FE method are compared. The maximum deviation of the deflection obtained by them is less than 5%, and the maximum strain error is less than 7%. These figures prove that all three methods have high precision in the elastic range. Compared SOSFs use a different shear keys with the same grid size and chords, the maximum Mises stress is reduced by 55.9% and the maximum displacement is reduced by 36.1%. The new shear key imparts the structure with improved bearing capacity and safety margin.

Keywords

Flanged cruciform section shear key; steel open-web sandwich floor; static test; intersection beam analogy method; finite element analysis.

Graphical Abstract

1 INTRODUCTION

In recent years, multi-layer and large-span buildings in China have been rapidly increasing due to the influence of social production demand and limited land supply. The steel-concrete composite space grid box structure composite invented by our team solves this problem very well (Ma et al. 2006).

The structure consists of SOSFs and steel grid frame walls (Xu et al. 2016) (Fig. 1). SOSF, an important part of the structure, is composed of a reinforced concrete (RC) floor slab, top chords, bottom chords, and shear keys (Fig. 2a). Studs are provided as a connecting member between the RC floor slab and the top chords.
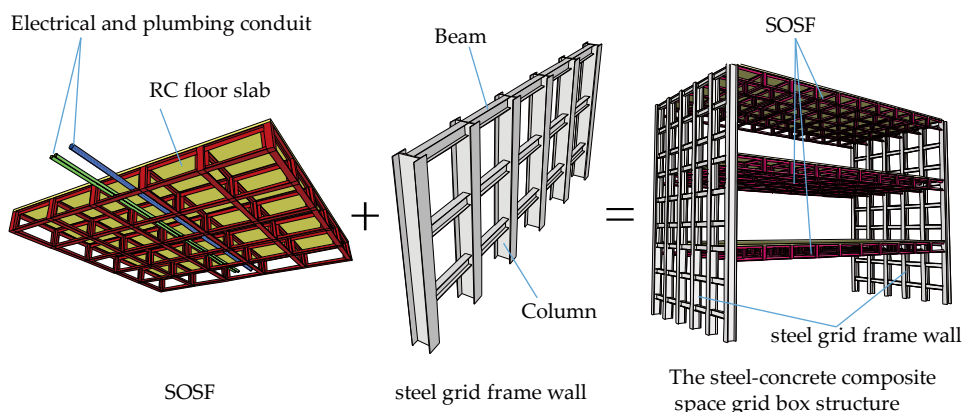

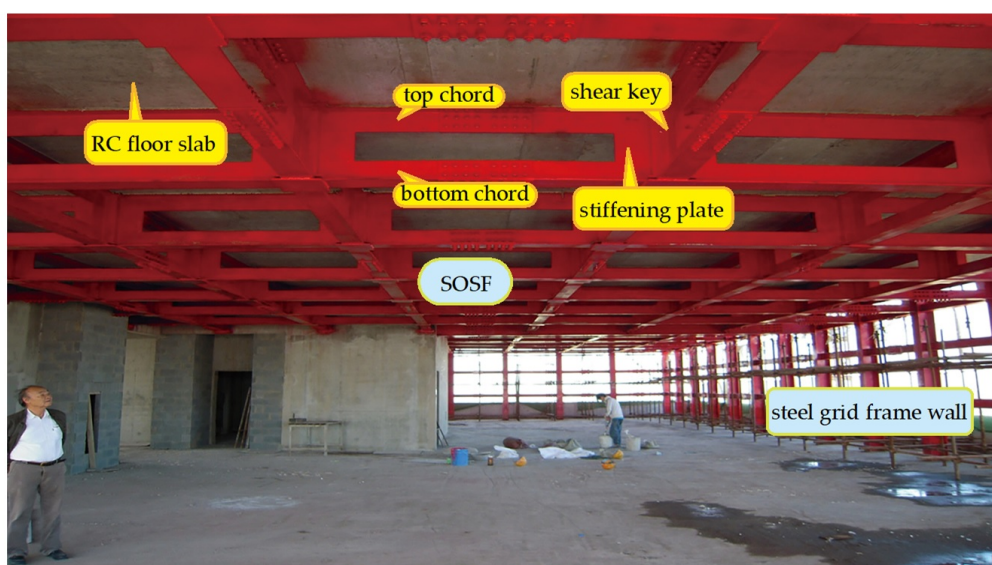
Figure 1. Components of the steel–concrete composite space grid box structure.

(a)

(b)

(c)

Figure 2. Application: (a) Tangshan Jianhua Engineering Quality Inspection Co., Ltd. Research and Testing Center Building; (b) Two-story large-span stadium in Mianyang Fule School, Sichuan Province; (c) Four-story large-span industrial plant in Jiuhua Innovation Industrial Park, Hunan Province.

The SOSF has the following advantages:

- The steel beam section height of the traditional steel–concrete composite beam structure ranges from span/10 to span/18. The larger the span, the larger the self-weight of the structure, the greater the ratio of the self-weight to the live load per unit area, and the lower the structural efficiency. The thickness of the SOSF structural layer ranges from span/25 to span/30. The structure hollow rate is 50%–60%. Compared with a traditional composite beam, the SOSF has lighter self-weight, smaller structural layer thickness, and better structural efficiency.

- Water and electricity pipes can pass through the space between the top and bottom chords, further reducing the structural thickness of the floor.

- SOSF can be constructed quickly through factory-prefabricated and on-site integrated assembly construction methods (Wei et al. 2008).

The research team studied the comprehensive mechanical properties of the SOSF. For example, Luan (Luan et al. 2016; Luan et al. 2017) studied the deflection distribution, stress response, and failure mechanism of the SOSF under load through scale model and field tests and found that the structure offers satisfactory structural performance. Chen (Chen et al. 2018) studied the seismic characteristics, deformation curves, inter-layer displacement, top-level displacement, and brittleness curves of SOSF by numerical simulation. Their results showed that the structure has large stiffness and greatly reduces seismic action. Bai and Ma (2018) conducted a dynamic elastoplastic analysis using time history analysis and found that the inter-layer displacement and inter-layer displacement angle of SOSF satisfy the standard requirements and have good ductility, dynamics, and seismic performance. Yang (Yang et al. 2013) used the scale model test and the FE method to study the mechanical properties and dynamic characteristics of the assembled monolithic SOSF structure. Their results indicated that the structure has excellent overall stiffness and high safety margin.

The above studies show that the structure has good comprehensive mechanical properties.

Given the above advantages, the SOSF has been applied in several pioneering industries and public buildings (Fig. 2).

Shear keys play a key role in SOSF. Most existing SOSFs use a square tube shear key. Liu (Liu et al. 2017) showed through the FE study that the square steel tube shear key has uneven stress distribution and evident stress concentration. When a stiffening plate was added to improve the stress state of the shear key, it effectively reduced the stress in the shear key and ensured its overall deformation characteristics, which substantially improved the overall bearing capacity of the structure. To further study the mechanical properties of the shear key, Shang (Shang et al. 2019) and Bai (Bai et al. 2018) designed full-scale shear key specimens and simulated cases under pure shears. The experimental results were compared with the simulations separately. When the stiffener plate was not provided, a stress concentration area at the joint of the chord and the shear key occurred during the loading process, and the yield of the steel first occurred in this area. Thus, the setting of the stiffener plate considerably improved the shear stiffness of the shear key. Jiang (Jiang et al. 2019) designed two full-size shear key test pieces of different joint forms and studied the seismic performance of the shear key. The stiffening plate was found to be effective for achieving a bearing capacity with high stiffness but was not conducive for absorbing and dissipating energy well.

Increasing the stiffening plate still does not fundamentally solve the problem of the non-smooth transmission of force in the shear key. It increases the bearing capacity and rigidity but also reduces energy consumption, which is not conducive to earthquake resistance.
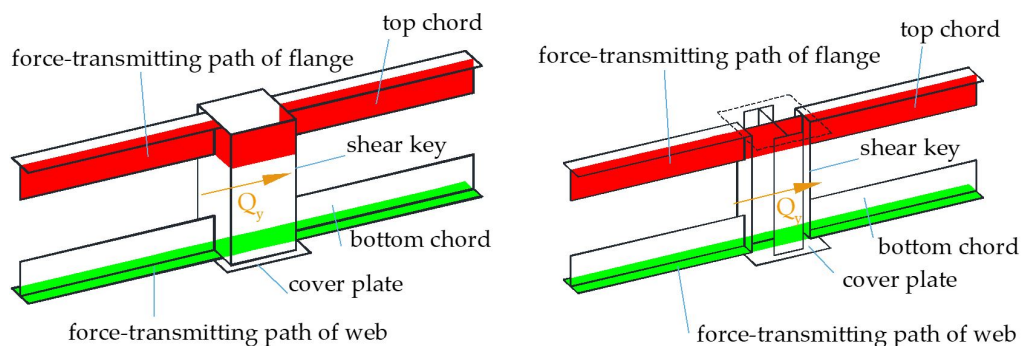
Figure 3. Force-transmitting path: (a) STSK; (b) FCSK.

The use of a new FCSK instead of STSK is proposed to solve the above problems and further improve the carrying capacity of the structure. When the square steel shear key is subjected to the shear force Q_y, the shear force Q_y between the two grids on the flange can be directly transmitted through the cover plate (green area in Fig. 3a). Given the hollow

construction of the square steel tube, the force transmission path on the web is not straightforward (red area in Fig. 3a). When the shear key is changed to a flanged cruciform shape section, the force transmission path of the new structure is more direct than that of the STSK (red area in Fig. 3b). This new type of shear key is a special-shaped shear key also known as FCSK. The entire structure is named as SOSF with FCSK and a Chinese patent has been applied for it (Shen et al. 2019).

For the new structure, we carried out a field test progam, gave a continuous analysis method, namely IBAM, and established a FE model. IBAM considers the influence of the finite shear stiffness of the Vierendeel beam. In FEM, shell and beam elements are selected for modeling. A half-scale test model is designed to verify the construction method and theoretical analysis results.

2 TEST PROGRAM

2.1. Structural model

A half-scale SOSF with FCSK test model is established in the Key Laboratory of Structural Engineering of Guizhou Province.

Figure 4 shows a 1 × 5 grid SOSF that is simply supported. The construction process is as follows.

First, 12 individual FCSKs are produced by welding two H-shaped steels and two cover steel plates. H-shaped steel uses laser to cut two slits in advance. The width of the slit is 1 mm thicker than the wall thickness of the H-shaped steel web. The length of the slit is half the total height of the web. Two H-beams are inserted through the slit pair. The final step is to fully weld the four parts (2 H-beams and 2 cover steel plates) into a complete FCSK (Figs. 4a and 4b) using the auxiliary line.

Second, the shear keys are connected by a full-weld connection through T-shaped chords to form a spatially coordinated SOSF system. Figure 4c shows a five-grid simplified mechanics model of the structure. The lateral length of the structure is *a*, and the longitudinal length is *5a*, which is divided into five grids. The length ratio of the long side to short side is 5. Thus, the structure is calculated with a one-way force structure. Owing to the symmetry of the structure, only the 1/4 structure and the corresponding A and B shear keys are analyzed.

Third, the SOSF is placed directly on the round steel support shown in Figure 4e. A square plate is placed between the round steel support and the concrete column. The square plates are directly anchored to the concrete column by expansion bolts. The square plate connects to the round steel by welding. When the test model is installed, the pre-made steel frame is placed directly on the round steel by a 10/3.2t bridge crane (Figs. 4f). A complete SOSF system is formed by pouring RC on the SOSF. The steel frame and the concrete slab are connected by a stud connection, as shown in Figure 4h.

This study examines the steel frame with a relatively simple structure as shown in Figure 4f, which does not consider the influence of the RC floor slab. Subsequent research will be carried out after concrete is poured on the structure.

Design test models in combination with commercially available steel profiles. The strength and stability requirements of components and joints of the engineering design were taken into consideration during selection to avoid structural failure mode differences between engineering applications and scale model tests. The cross-sectional dimensions of each component are shown in Figure 5. The FCSK has a flange thickness of 7 mm and a width of 75 mm. The web is 5 mm thick and 150 mm wide. The shear key height *h* is 200 mm. The grid size a is 1000 mm. The top and bottom chords are composed of T-shaped steel with a cross-sectional dimension of T75 mm × 75 mm × 5 mm× 7 mm and a length of 850 mm. The long axis direction has five grids. The structural thickness of the SOSF is span/25 which is 200mm. Two 1600 mm 10# I-beams, with a section measuring 100 mm × 68 mm × 4.5 mm, are installed on the shear key of the SOSF's third grid to facilitate loading. The steel I-beam is connected to the cover plate of the shear key by spot welding. During the loading process, the loading iron blocks are placed in a 1.5 m × 1.5 m loading basket, which is directly hoisted on the I-beam by a crane to achieve static loading (Fig. 6). There is an 8 mm gap between the I-beam and the top chord flange. Under the maximum design load of 9.6 kN, the maximum vertical displacement of the I-beam occurs in the midspan with a deformation of 0.018 mm, which is far less than 8 mm. Thus, the I-beam will not come into contact with the top chord under the design load, and the loading area can be simplified to the red area of the shear key's cover plate, as shown in Figure 5.

The displacement data are collected by SICK Company's AOD5-N1 laser displacement transducers (DTs). The strain data are collected using a Dong Hua DH3819 wireless static data acquisition instrument. The measured points are concentrated in the 1/4 range of the structure to take advantage of its structural symmetry. Eight strain gauges (A1–A8) are attached to the edges of the web in the top and bottom chords. Two laser DTs are fixed below the center point of shear keys A and B to measure the deflections. Figure 6 displays the position of the DTs and strain gauge.
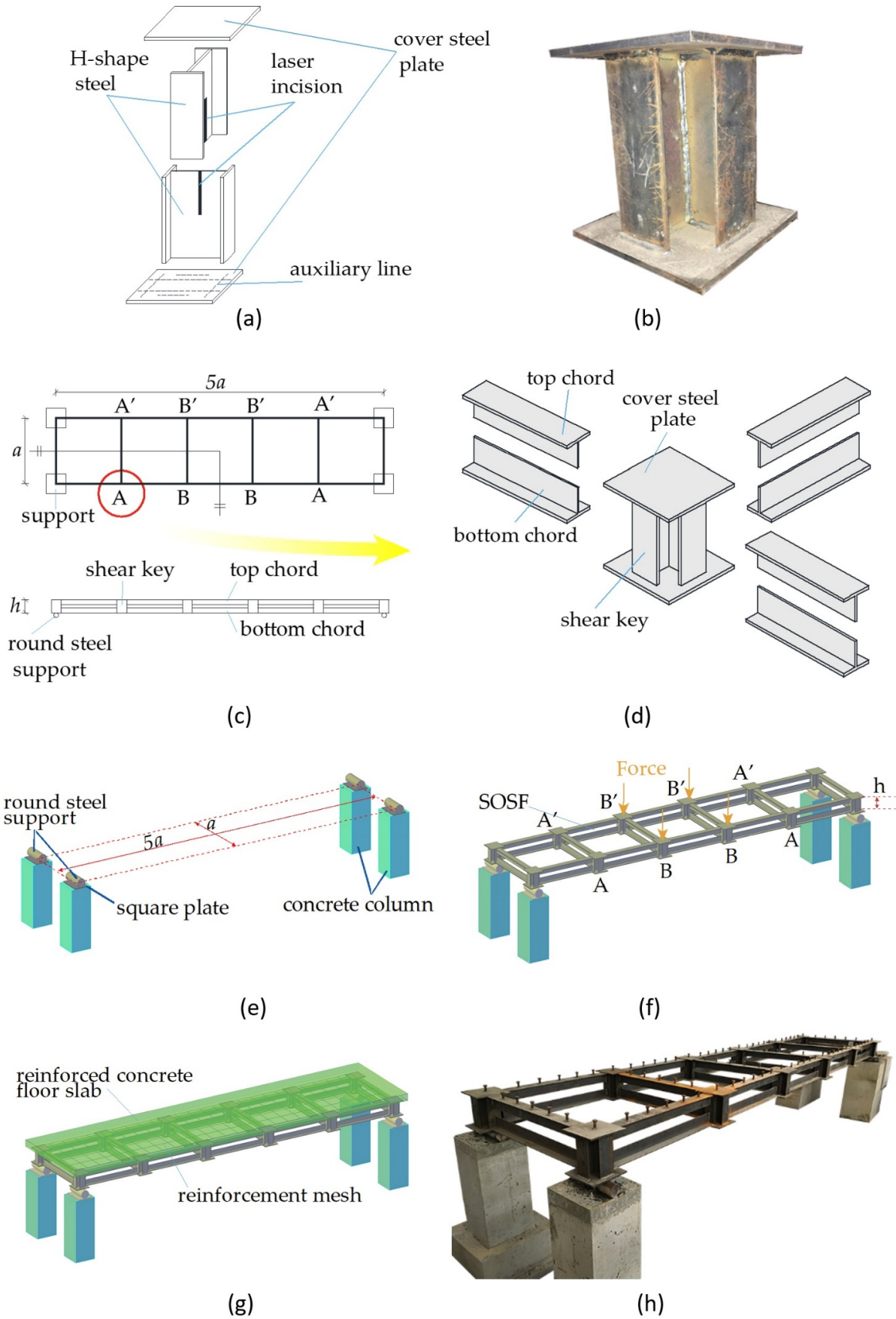
Figure 4. Configuration of the test model: (a) Assembly diagram of the FCSK; (b) Photo of FCSK; (c) Plan and front view of a five-grid SOSF structure; (d) Assembly diagram of the FCSK and chords; (e) Support; (f) SOSF; (g) SOSF with RC floor slab; (h) Photo of the test model.
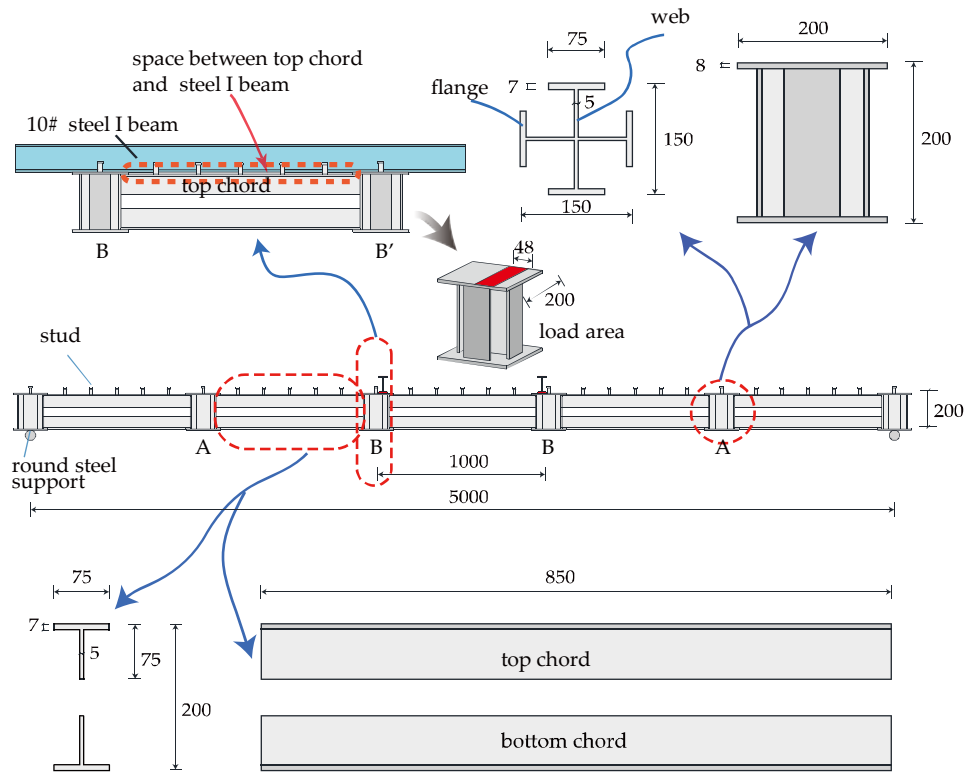
Figure 5. Geometrical dimensions of the shear key, top chords, and bottom chords.
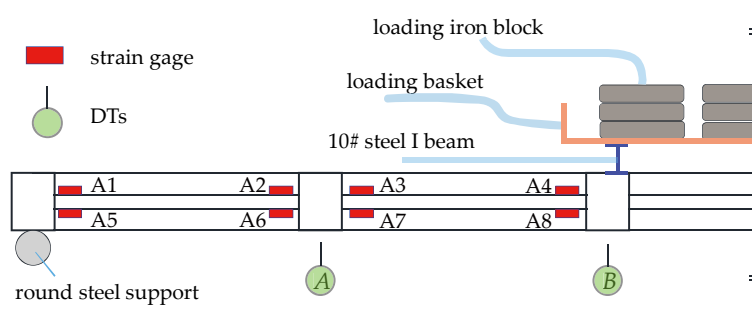

Figure 6. Experimental device

2.2 Material properties
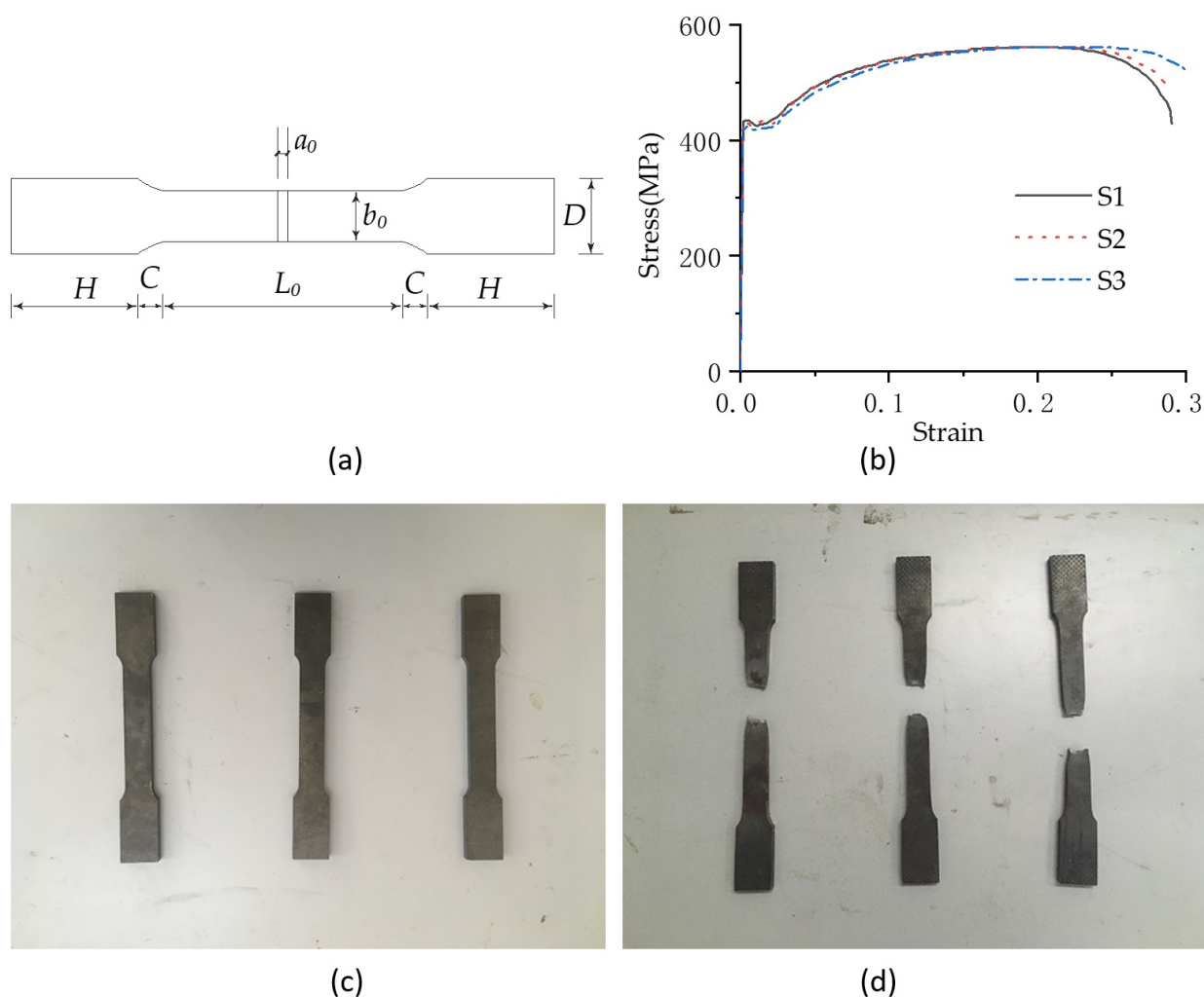

(a)

(b)

(c)

(d)

Figure 7. Material property test: (a) Test specimen details; (b) Stress–strain curves of Q235; (c) Before tensile testing; (d) After tensile testing.

The chords and shear keys are made of Q235 steel. Cut three test pieces from the flange part of the remaining material for the test model and perform the tensile test. The test sample and detailed dimensions are shown in Figure 7a. The elastic modulus (E_s), yield strength (f_y), ultimate strength (f_u) and yield ratio (f_u/f_y) are tested and measured. Figure 7b illustrates a stress–strain curve comparison of the three samples. Figure 7c presents the test piece before stretching, and Figure 7d illustrates the test piece after the tensile fracture. The results of the average test of the three test pieces are shown in Table 1.

Table 1 Material properties of steel

	S1	S2	S3
H(mm)	50	50	50
C(mm)	10	10	10
L_0(mm)	95	95	95
a_0(mm)	7	7	7
b_0(mm)	20	20	20
D(mm)	30	30	30
f_y(MPa)	424.0	424.3	415.7
f_u(MPa)	560.9	561.5	561.7
E_s(MPa)	203000	210000	209000
f_u/f_y	1.32	1.32	1.35

2.3. Loading procedure

A bending test is conducted at the SOSF as described above. The loading iron basket weighs 78 kg, the 10# steel I-beams weigh 17.92 kg each, and the loaded iron blocks weigh 20.4 kg each. Twelve blocks are present per layer, with each layer weighing 244.8 kg (gravity load is 2.4 kN). An empty loading basket is pre-placed on the 10# steel I-beam. After 30 min of rest, the laser displacement meter data acquisition system and the strain acquisition system are balanced to zero, and data are recorded. The test is designed as a non-destructive test because the concrete should be poured on the test model to proceed to the next experimental study after completion of the experiment. The maximum design load during the test is 9.6 kN (4 layers x 12 pieces of loading iron block). As shown in Table 2, the loading is performed in three stages. The first level loads two layers of iron, and the next two stages load a layer of iron. Each loading phase lasts approximately 30 min. Figure 8 shows the loading scene photo.

Table 2 Load stages

Initial stage	First stage	Second stage	Third stage
Empty iron basket	4.8 kN	7.2 kN	9.6 kN

Figure 8. Loading in progress: (a) Initial state; (b) Loading process.

2.4. Discussions of the test results

As shown in Figure 6 above, two points (A and B) are selected to measure the deflection data, and eight points (A1 to A8) are selected to measure the strain data in the test. Anomalous data are collected at the fifth and eighth measuring points, which indicate that the strain gauges may be faulty. The vertical deflections and strains measured under different load stages are plotted in Figure 9.

During the entire test, no macroscopic damage of the test model, local buckling of the steel profile, and weld cracking are observed. The strain and displacement of the top and bottom chords and shear key show similar linear changes. The maximum strain of each measuring point remains below the yield strain of the material. Thus, the test model is in an elastic working state during the test without plastic deformation and damage. Under the load of 9.6 kN, the deflection test value is 5.508 mm, which is 1/908 of the span, indicating that the structure has good overall stiffness.
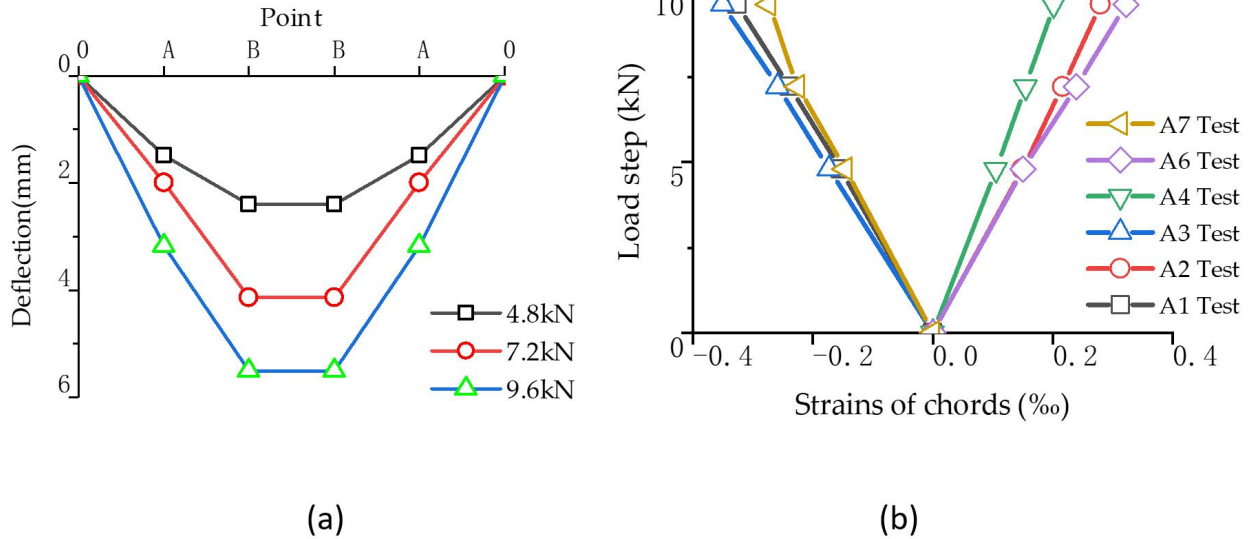
(a)   (b)

Figure 9. (a)Deflection of the floor; (b) Average strains of points

3 CONTINUOUS ANALYSIS METHOD

3.1. IBAM

The continuous analysis method of the SOSF system is divided into the IBAM (Dong et al. 1992; Makowski 1981) and pseudo-plate method (Huang et al. 1997, 1998). After the equivalent moment of inertia (I_{eq}) and equivalent shear stiffness (C_{eq}) of the equivalent beam in each direction are determined, the deflection can be calculated by the IBAM. The internal force is calculated according to the structural mechanics. This article uses this method.

The following basic assumptions are used in the calculation:

- The number of grids in the direction of the force cannot be less than five.

- The effects of twisting are ignored.

This test model can be further simplified:

- The force of the four-point support unidirectional force structure in the short-side direction is almost negligible. The structure can be simplified by a plane mechanics model (Fig. 10).

According to the above assumption, h is the structural layer thickness, and a is a calculation unit length in the mechanics model (Fig. 10a). The cross-sectional area of the top chord is A_1, the bending rigidity is EI_1; the cross-sectional area of the bottom chord is A_2, the bending rigidity is EI_2; the cross-sectional area of the shear key is A_v, and the bending rigidity is EI_v. The SOSF is replaced with an equal solid beam, with a unit height of h and a length of a (Fig. 10b).

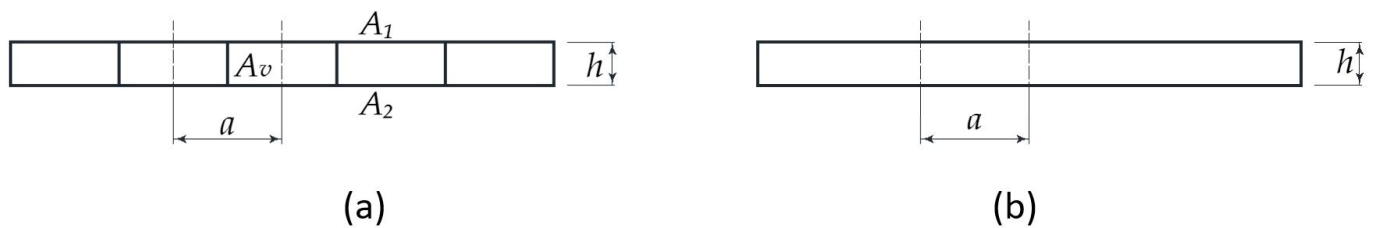(a)   (b)

Figure 10. Mechanical model: (a) SOSF; (b) Equal solid beam.

Rotation angles θ_a and θ_b are produced under the action of a unit bending moment applied to the SOSF and the equal solid beam of unit length a, respectively. They are equal under the equivalent replacement condition, that is, $\theta_a = \theta_b$. The top and bottom chords generally have the same cross-section design lead to $A_1 = A_2$. The calculation of I_{eq} is:

$$I_{eq} = \frac{A_1 A_2}{A_1 + A_2} h^2 = \frac{1}{2} A_1 h^2 \tag{1}$$

The SOSF unit is subjected to shear forces V_1 and V_2 and is balanced with the horizontal force H in the direction of the top and bottom chords (Fig. 11a). The unit receives a total shear force of $V = V_1 + V_2$. The corresponding shear forces and horizontal forces of the equivalent solid beams are V and H, respectively (Fig. 11b). The stress distribution of the equal solid beam unit is the same as that stated in the Reissner hypothesis of sandwich beam (Reissner 1947), that is, the shear stress remains constant along the cross-sectional height of the beam element.
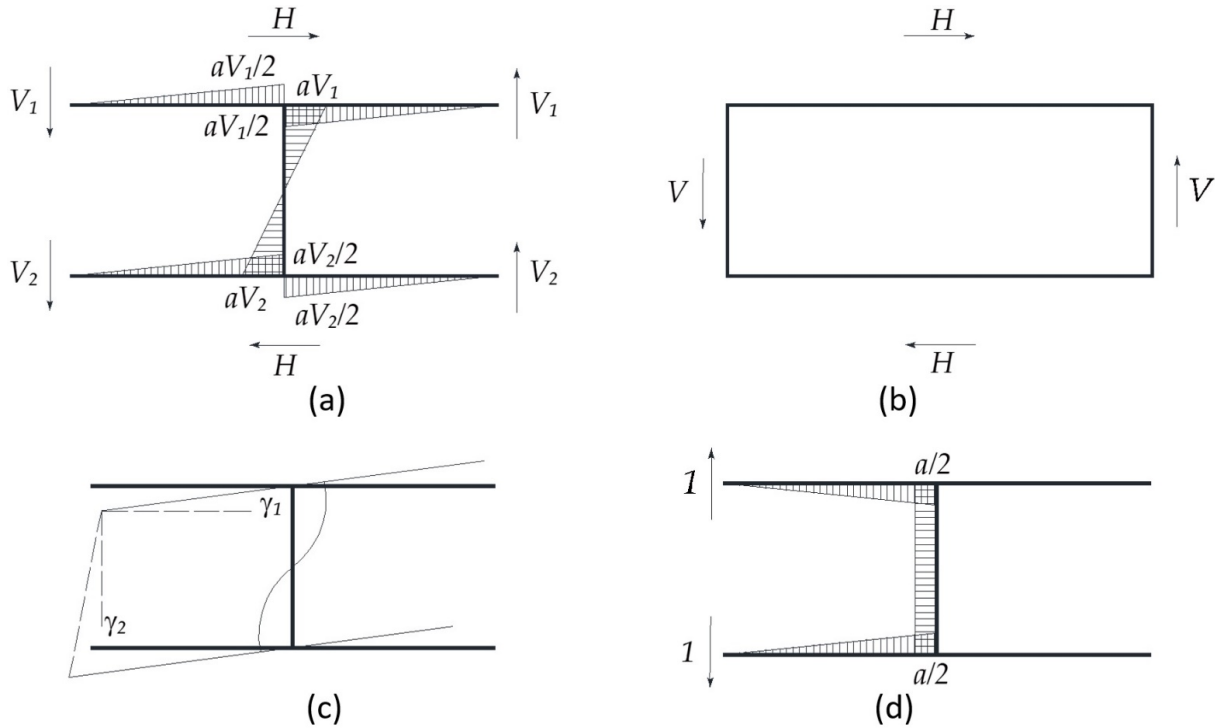

Figure 11. Shear deformation between chords: (a) Shear force and bending moment under shear force; (b) Equal solid beam; (c) Shear deformation; (d) Moment diagram of unit force acting on the top and bottom chords.

The shape of the SOSF unit after deformation is shown in Figure 11c. γ_1 represents the deviation of the end of the top or bottom chord from the original position, γ_2 denotes the deviation of the end line connecting the top or bottom chord from the vertical line, and γ_v refers to the deformation of the shear key itself. The total shear deformation is as follows:

$$\gamma = \gamma_1 + \gamma_2 + \gamma_v \tag{2}$$

The bending moment distribution of the unit forces acting on the top and bottom chords is shown in Figure 11d. Applying a diagram multiplication method with Figures 11a and 11d can obtain the vertical relative displacement $\delta_{1,2}$ of the top and bottom chords:

$$\delta_{1,2} = \frac{1}{EI_1}\left[\frac{1}{2}\cdot\frac{aV_1}{2}\cdot\frac{a}{2}\cdot\frac{2}{3}\left(-\frac{a}{2}\right)\right] + \frac{1}{EI_2}\left[\frac{1}{2}\cdot\frac{aV_2}{2}\cdot\frac{a}{2}\cdot\frac{2}{3}\cdot\frac{a}{2}\right] + \frac{1}{EI_v}\left[\frac{1}{2}\cdot aV_2\cdot\frac{V_2 h}{V_1+V_2}\cdot\frac{a}{2}\right] + \frac{1}{EI_v}\left[\frac{1}{2}\cdot aV_1\cdot\frac{V_1 h}{V_1+V_2}\cdot\left(-\frac{a}{2}\right)\right]$$

When no relative displacement occurs between the top and bottom chord, $\delta_{1,2} = 0$. When the same section size for the chord sections is used ($I_1 = I_2$), the following is obtained:

$$V_1 = \frac{h / I_v + a / 6I_2}{h / I_v + a / 6I_1} V_2 = V_2 = \frac{1}{2}V \tag{3}$$

The unit exhibits a zero external torque balance condition, that is, $Va-Hh = 0$:

$$H = \frac{a}{h} V \tag{4}$$

Shear deformation of the shear key itself is computed by

$$\gamma_v = \frac{aV}{kGA_v h^2}$$

where k represents the shear stress distribution coefficients, and G is the shear modulus.

According to the above formula, the total shear deformation γ is calculated by the diagram multiplication method as

$$\gamma = \gamma_1 + \gamma_2 + \gamma_v = \frac{a^2}{12(V_1 + V_2)}\left(\frac{V_1^2}{EI_1} + \frac{V_2^2}{EI_2}\right) + \frac{ah}{3EI_v(V_1 + V_2)^2}(V_1^3 + V_2^3) + \frac{aV}{kGA_v h^2} = \frac{a^2 V}{24EI_1} + \frac{ahV}{12EI_v} + \frac{aV}{kGA_v h^2}$$

According to the definition of the linear stiffness i, setting $i_1 = EI_1/a = EI_2/a$ and $i_v = EI_v/h$, the above formula is simplified as follows:

$$\gamma = \frac{aV}{24i_1} + \frac{aV}{12i_v} + \frac{aV}{kGA_v h^2} \tag{5}$$

Under the action of the shear force V and the corresponding equilibrium shear force H, the shear deformation γ' of the equal solid beam is calculated as follows:

$$\gamma' = \frac{V/h}{G} = \frac{V}{C_{eq}} \tag{6}$$

where C_{eq} represents the equivalent shear strength.

Setting $\gamma = \gamma'$, the C_{eq} is

$$C_{eq} = \frac{1}{a\left(\dfrac{1}{24i_1} + \dfrac{1}{12i_v} + \dfrac{1}{kGA_V h^2}\right)} \tag{7}$$

The equivalent shear strength is compared with the formula given by Křístek (1979). and Bakht and Jaeger (1985) when the shear key is a conventional square steel tube. The condition is obtained when the top and bottom chord sections are the same, and the influence of the concrete slab is not considered. The calculation results are consistent (Xiao et al. 2000).
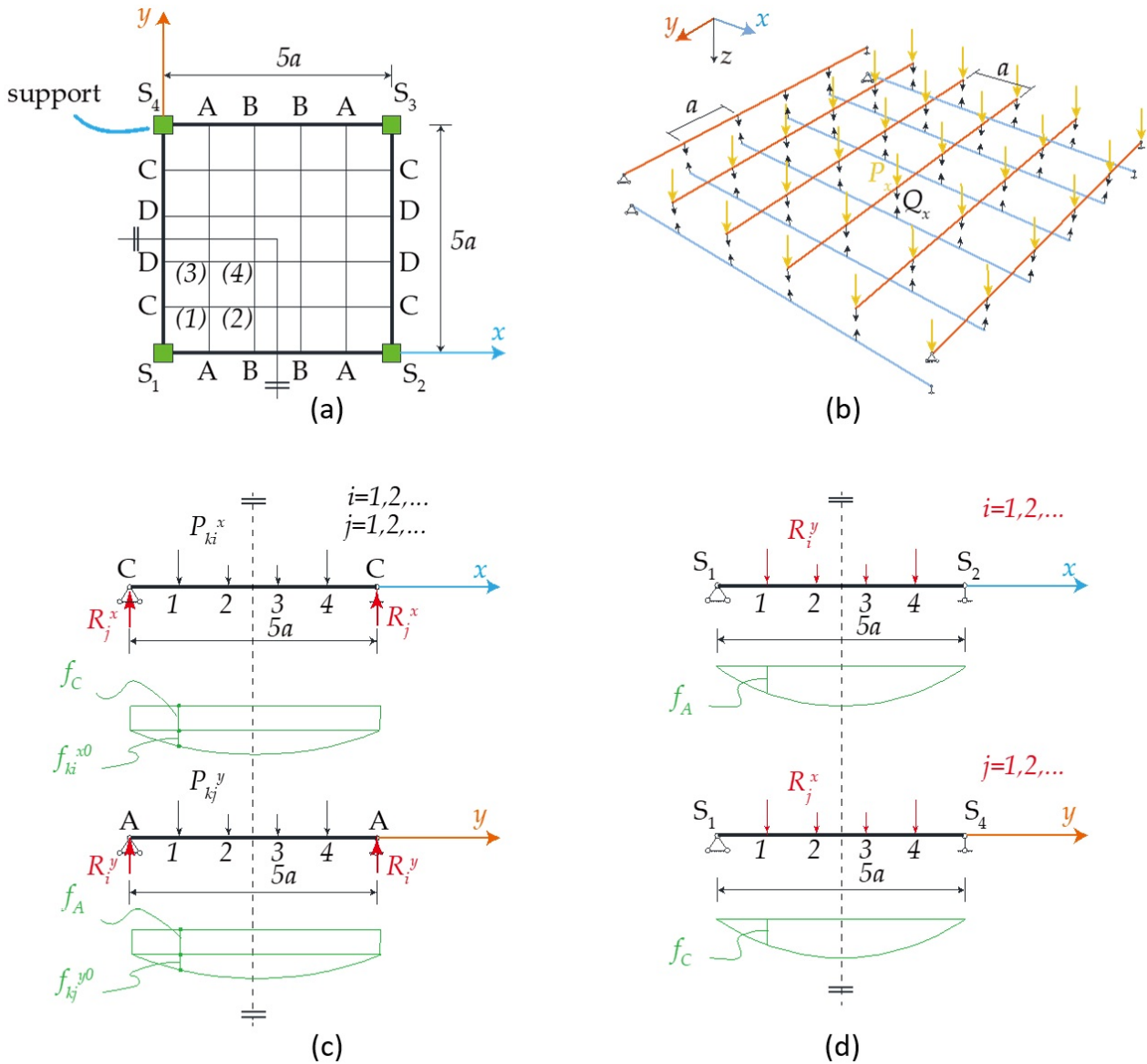
Figure 12. Mechanical model: (a) Overall number; (b) Node load assigned to the beam; (c) Edge beam's local number and calculation diagram; (c) Intermediate beam's local number and calculation diagram.

With the SOSF replaced with the equal solid beam by I_{eq} and C_{eq}, the general calculation steps of the IBAM is introduced by taking a four-point-support 5 × 5 grid SOSF structure under uniform load as an example. The nodes of the intersection beam in the whole structure are numbered according to the symmetry, denoted by k (Fig. 12a). The nodes of the separate beam in a local structure are numbered and denoted by i and j (Figs. 12c and d). The basic assumptions of the calculation are as follows:

- Assuming that the nodes of the intersection beams are all rigid connections, uniform loads are simplified into the node load $P_{k1} = P_{k2} = ... = P_k = qa^2$.

- Assuming that the intersection beam nodes are connected by rigid only-tension links, the links are cut off to obtain an unknown force, Q_k (Fig. 11b). The corresponding node loads assigned to the x-direction beams are P_{ki}^x (i = 1, 2, ...) and those assigned to the y-direction beams are P_{kj}^x (j = 1, 2, ...) (Fig. 11c). According to the principle of equilibrium of nodal forces, $P_{ki}^x = P_k - Q_k$, $P_{kj}^x = Q_k$; that is $P_{kj}^y = P_k - P_{ki}^x$.

- Assuming that the intersection nodes have no relative deformation, the vertical deflections of the corresponding k node of the x- and y-direction beams are equal, that is, $f_{ki}^{x} = f_{kj}^{y} = f_{k}$.

The counter-forces acting on the x- and y-direction beams are R_{j}^{x}, R_{i}^{y}, respectively. The following can be obtained:

$$R_{j}^{x} = \frac{1}{2}(P_{k} + \sum_{i=1}^{m} P_{ki}^{x}), R_{i}^{y} = \frac{1}{2}(P_{k} + \sum_{j=1}^{n} P_{kj}^{y}) = \frac{1}{2}P_{k} + \frac{1}{2}\sum_{j=1}^{n} P_{k} - \frac{1}{2}\sum_{j=1}^{n} P_{ki}^{x}.$$

The deflection of each point on the boundary beam S$_1$S$_2$ is determined according to the diagram multiplication method:

$$f_{A} = \sum_{i=1}^{m} R_{i}^{y} \delta_{Aj}^{(S_1 S_2)} = \sum_{i=1}^{m} [\frac{1}{2}P_{k} + \frac{1}{2}\sum_{j=1}^{n} P_{k} - \frac{1}{2}\sum_{j=1}^{n} P_{ki}^{x}] \cdot \delta_{Aj}^{(S_1 S_2)} = \frac{1}{2}[\sum_{i=1}^{m} P_{k} + \sum_{i=1}^{m}\sum_{j=1}^{n} P_{k} - \sum_{i=1}^{m}\sum_{j=1}^{n} P_{ki}^{x}] \cdot \delta_{Aj}^{(S_1 S_2)}$$

where $\delta_{Aj}^{(S_1 S_2)}$ represents the deflection value of point A obtained by the diagram multiplication method of S$_1$S$_2$ under the action of $R_{i}^{y} = 1$. Similarly, the deflection of each point on the boundary beams S$_1$S$_4$ can be obtained as follows:

$$f_{C} = \frac{1}{2}[\sum_{j=1}^{n} P_{k} + \sum_{j=1}^{n}\sum_{i=1}^{m} P_{ki}^{x}] \cdot \delta_{Cj}^{(S_1 S_4)}$$

$$f_{ki}^{x} = f_{C} + f_{ki}^{x0} = \frac{1}{2}[\sum_{j=1}^{n} P_{k} + \sum_{j=1}^{n}\sum_{i=1}^{m} P_{ki}^{x}] \cdot \delta_{Cj}^{(S_1 S_4)} + \sum_{i=1}^{m} P_{ki}^{x}\delta_{ki}^{x} \tag{8a}$$

$$f_{kj}^{y} = f_{A} + f_{kj}^{y0} = \frac{1}{2}[\sum_{i=1}^{m} P_{k} + \sum_{i=1}^{m}\sum_{j=1}^{n} P_{k} - \sum_{i=1}^{m}\sum_{j=1}^{n} P_{ki}^{x}] \cdot \delta_{Aj}^{(S_1 S_2)} + \sum_{i=1}^{n} P_{kj}^{y}\delta_{kj}^{y} \tag{8b}$$

The above formula is substituted into the previous assumption $f_{ki}^{x} = f_{kj}^{y}$, that is (8a) = (8b), thus finishing the following formula:

$$\frac{1}{2}[\sum_{j=1}^{n} P_{k} + \sum_{j=1}^{n}\sum_{i=1}^{m} P_{ki}^{x}] \cdot \delta_{Cj}^{(S_1 S_4)} + \sum_{i=1}^{m} P_{ki}^{x}\delta_{ki}^{x} = \frac{1}{2}[\sum_{i=1}^{m} P_{k} + \sum_{i=1}^{m}\sum_{j=1}^{n} P_{k} - \sum_{i=1}^{m}\sum_{j=1}^{n} P_{ki}^{x}] \cdot \delta_{Aj}^{(S_1 S_2)} + \sum_{i=1}^{n} P_{k}\delta_{kj}^{y} - \sum_{i=1}^{n} P_{ki}^{x}\delta_{kj}^{y} \tag{9}$$

The SOSF has k intersection nodes to write k equations shaped like Formula (9). The equation is solved to obtain the nodal load P_{ki}^{x} in the x-direction. Formula (8a) or (8b) is introduced to determine the deflection f_k of each point in the SOSF.

3.2. Numerical example

After the SOSF in the foregoing test is replaced with an equal solid beam, the calculation model shown in Figure 13 is simplified according to the symmetry of the structure. The Chinese standards and test results are followed to obtain the relevant physical quantities shown in Table 3:
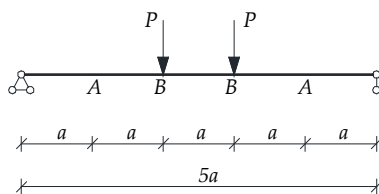
Figure 13. Calculation model

Table 3 Physical quantities in numerical example

Physical quantity	Unit	Description	Value
E	N/mm²	Young's modulus	207000
μ	-	Poisson's ratio	0.3
G	N/mm²	Shear modulus	79000
A_1	mm²	area of top chord	935
I_1	mm⁴	inertia coefficient of top chord	431000
A_v	mm²	area of shear key	3715
I_v	mm⁴	inertia coefficient of shear key	7620000
k	-	shear stress distribution coefficients	2.285
a	mm	grid size	1000
h	mm	structural layer thickness of the SOSF	200

When Formulas (1) and (7) are substituted, $I_{eq} = 1.87 \times 10^7 mm^4$ and $C_{eq} = 2.08356 \times 10^6 N$. The deflection at each point can be obtained by bringing the three-stage load in the test into the previous calculation method, as shown in Figure 14.
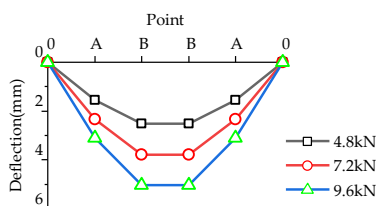

Figure 14. Calculation result of deflection
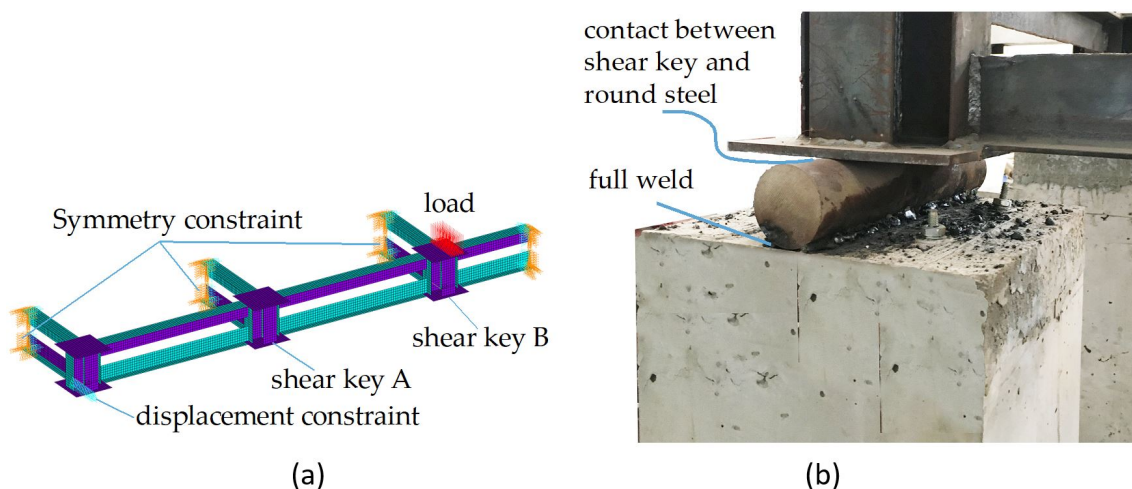
4. FE MODEL

(a)

(b)

Figure 15. (a) FE model; (b) Support detail photo.

In the FE model, the 1/4 structure in Figure 15a is analyzed on the basis of the symmetry of the structure. The orange area is the symmetric constraint. The SOSF with the FCSK is composed of a thin-walled member. Therefore, selected SHELL181 elements in Ansys19.0 have high accuracy, and all the grid size is 12.5 mm. Given that the whole steel frame is connected by welding, the FEM is selected by the common node modeling method. As shown in Fig. 15b, the round steel and the steel plate on the concrete support are connected by welding. The FCSK is directly placed on the round steel. They are only in a contact relationship and act on a straight line. The cyan triangle only indicates a displacement constraint present in the vertical direction. As shown in Figure 5, the load is directly applied to the red area in the FE model.

Considering that large models will be studied in the future, modeling with efficient beam elements will inevitably greatly reduce modeling and calculation time. To facilitate comparison, the beam element and shell element modeling are also used for comparison. The FCSK in the beam element modeling must be customized in advance.

5. COMPARISON OF RESULTS

5.1. Deflection

Table 4 compares the results for each measuring point A and B under the designed loading with three methods: IBAM, the measured values in the test program, and FE analysis values with shell and beam elements. The maximum error rate is then calculated.

Table 4 Physical quantities in numerical example

Measure point	Design load (kN)	Test	IBAM		FEM (beam)		FEM (shell)		Maximum Error rate
		Deflection (mm)	Deflection (mm)	Error rate	Deflection (mm)	Error rate	Deflection (mm)	Error rate	
A	0	0	0	-	0	-	0	-	-
	4.8	1.487	1.552	4.37%	1.478	0.61%	1.427	4.03%	4.37%
	7.2	2.247	2.328	3.60%	2.217	1.34%	2.14	4.76%	4.76%
	9.6	2.981	3.105	4.16%	2.957	0.81%	2.853	4.29%	4.29%
B	0	0	0	-	0	-	0	-	
	4.8	2.606	2.52	3.30%	2.658	2.00%	2.487	4.57%	4.57%
	7.2	3.839	3.78	1.54%	3.987	3.86%	3.73	2.84%	3.86%
	9.6	5.108	5.04	1.33%	5.316	4.07%	4.973	2.64%	4.07%

The maximum error rate of the IBAM, test, and FEM results reach 4.76%, which is less than 5%. Thus, the one-way forced SOSF with FCSK structure can use the formula given above to calculate deflection without considering the effect of the RC floor slab. The results show high precision within the elastic stage. The FE uses the beam and shell elements to establish a model error rate within 5%. Both elements, which can be arbitrarily selected according to the actual situation, show high precision. The FE simulation results fit the experimental findings well. The FE model can be used for further in-depth research.
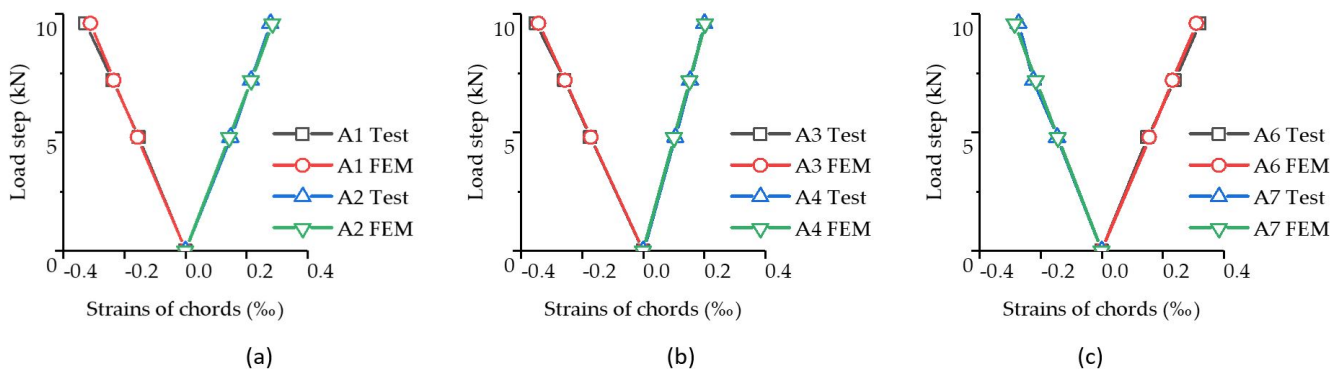
5.2. Strains

Figure 16. Load–strain curves.

Figure 16 is a comparison of the load–strain curve for the test and the FEM. The chord is always in an elastic working condition under the design load. The error rate of each point in the test data and FEM is kept below 5%, and the FEM can reflect the deformation of the test model.

5.3. Force distribution

Figure 17 shows the force distribution of chords and shear keys under 9.6 kN load. The top and bottom chords in the SOSF system are in compression–bending and tension–bending stress states, respectively. From the support to the span, the axial force gradually increases and the bending moment is gradually reduced. The stress distribution is relatively uniform. The shear key occurs mainly with the bending moment and shearing force, which gradually reduces from the support to the span. The FE analysis results show that the stress and strain distributions coincide with the experimental results. Thus, the FE analysis results are highly consistent with the test.
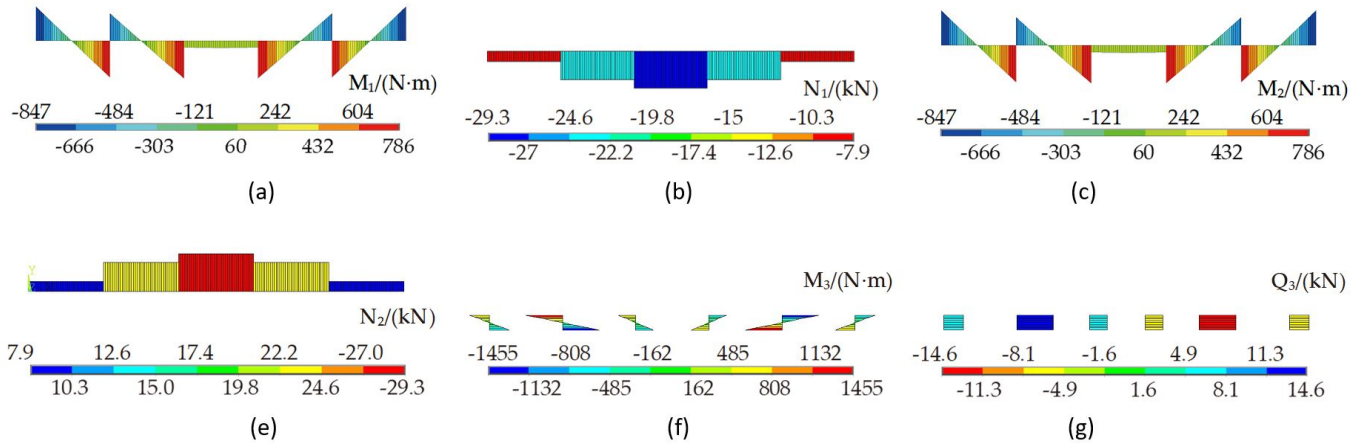

Figure 17. Internal force distribution (unit for force [kN] and unit for moment [N·m]): (a) Moment in the top chord; (b) Axial force in the top chord; (c) Moment in the bottom chord; (d) Axial force in the bottom chord; (e) Moment in the shear key; (f) Shear force in the shear key.

6. COMPARISON OF FCSK AND STSK

The carrying capacities of the SOSF with two forms of shear keys are compared. This experiment is a non-destructive test, and the maximum load is designed to be conservative at 9.6 kN. The FE of the linear elastic phase obtained in the previous conclusion is in good agreement with the experimental results. The FE is used to conduct an in-depth study on the carrying capacity of the structure. FCSK is replaced with STSK (150 mm × 150 mm × 6 mm) by the same amount of steel. Both SOSF models are 5000 mm × 1000 mm × 200 mm, and the dimension of the T-chords is exactly the same (Fig. 18).
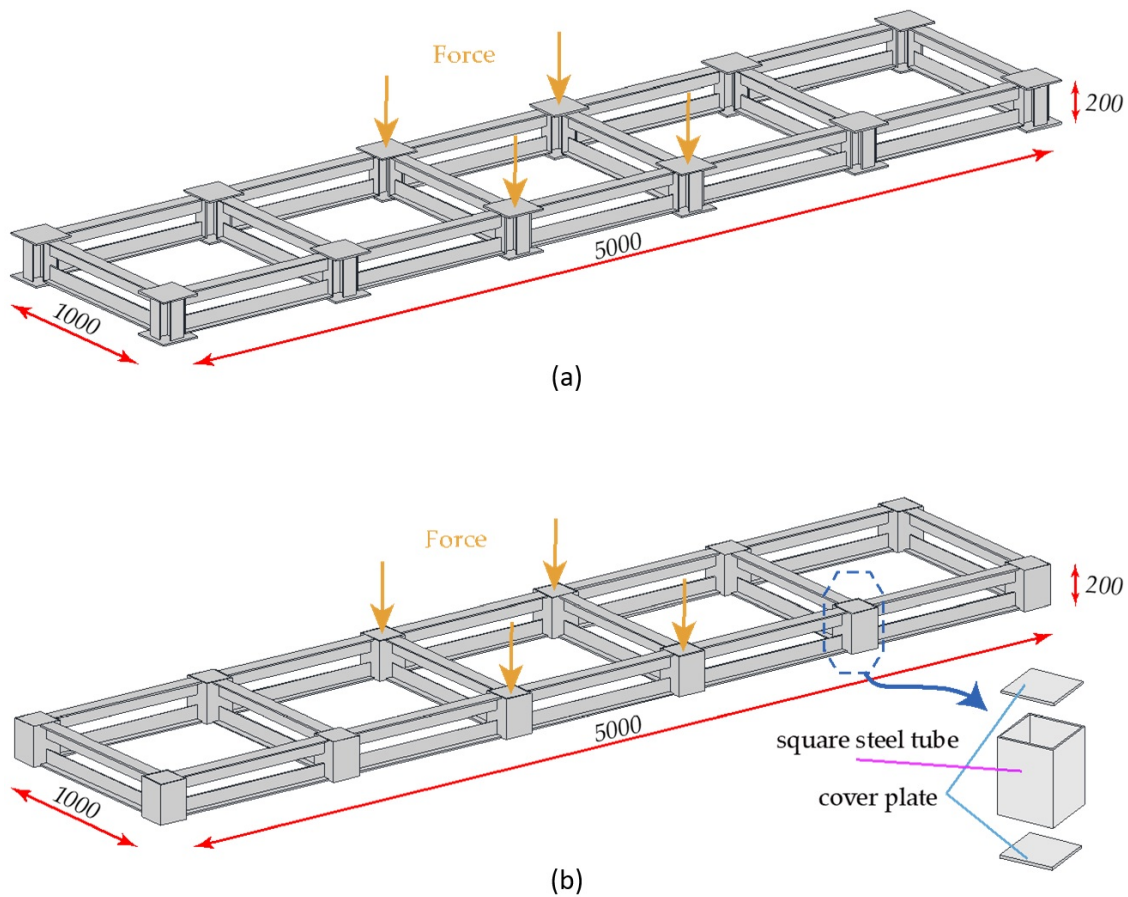
Figure 18. Two SOSF contrast models with different shear keys: (a) FCSK; (b) STSK.

The overall bearing capacity of the two models is compared. Ramped loads are applied to both models from 0 to obtain the maximum Mises stress–load curve and maximum deflection–load curve of the structure (Fig. 19). When the SOSF with STSK is loaded to 10.11 kN, the side wall of the shear key at the joint of the chord and the shear key reaches the design yield strength of the steel (235 Mpa). The stress concentration of the STSK is serious, whereas the stress distribution is not uniform. The maximum deflection of the structure is 7.89 mm. The maximum Mises stress of the FCSK is on the side of the T-section chord web near the shear key achieving 93.52 MPa under the same load. The new structure has a maximum deflection of 5.04 mm. Compared with the STSK, the new type of shear key reduced the maximum stress by 55.9% and the maximum deflection by 36.1%. When the load reaches 25.87 kN, the steel of the new structure reaches the design yield strength (235 Mpa) in the T-section chord web near the shear key. The new structural bearing capacity is increased 2.56 times, and the position of yielding is different. In comparison, the STSK is the shear key yielded first, and the FCSK is the chord yielded first. This result indicates that the shear key still has great reserves of structural stiffness during chord yielding. At this time, the deflection of the new structure is 12.89 mm, and the maximum relative displacement is $f_{max}/l = 1/388 < (1/300)$. The deflection satisfies the design requirements of Chinese codes. In summary, the new type shear key can significantly improve the load-bearing capacity and safety margin of the structure.
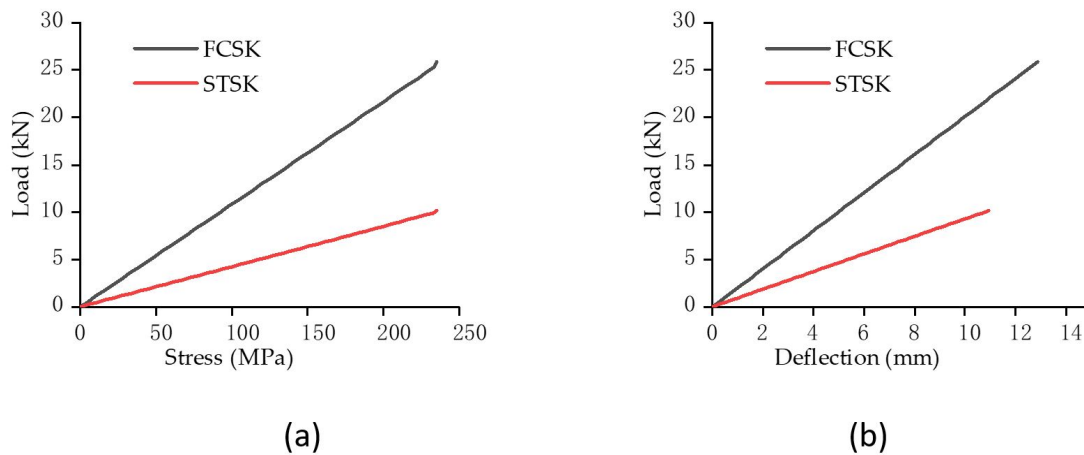
Figure 19. (a) Maximum Mises stress–load curve; (b) Maximum deflection–load curve.

7. DISCUSSION

As a newly proposed structural form, the SOSF with FCSK has no actual project and is currently only in the experimental and theoretical research stage. In the design, the fabrication and static loading test of the half-scale model are described in this paper. The theory and FE of the new structure are verified. Given the subsequent need to pour concrete to form a steel–concrete combined structure for further analysis, this study only designs loading in the elastic phase to study the mechanical properties. The increase in load-bearing capacity of the structure using the new-style shear key is evident. Correlation research, such as seismic and dynamic performance of the proposed structure, must be performed before it can be applied to actual projects. In existing projects, the steel members of the flanged cruciform section mainly appear in the form of columns. The stability (Naderian et al. 2019), shear stiffness, and torsion resistance of the flanged cruciform section column have been previously studied (Nasrabadi et al. 2013). The corresponding properties of the FCSK in the SOSF structure, especially the torsion resistance, still require the fabrication of separate components for further investigation.

Making a new-style shear key is more complicated than making a traditional one. However, because the steel flanged cruciform section column has been widely used in projects, it can be directly customized and fabricated as the new shear key in factories, greatly reducing the difficulty and time of production compared with the method used in the test. When combined with the already mature assembly method, the on-site welding operation can be greatly reduced, and the construction progress can be accelerated. However, given its high cost and complicated structure, the application of the SOSF adopting the new FCSK can realize its advantages in the application of large span and heavy load structures.

8. CONCLUSIONS

Test program, continuity analysis method, and FEM of the newly proposed SOSF with FCSK are performed. The results of the three are compared, and the new-style shear key is compared with the traditional STSK. The following conclusions are drawn.

1. An IBAM mechanical calculation model considering shear stiffness is established, and the test and corresponding FE models are designed for verification. Results show that the maximum deviation of the deflection values of the selected measuring points under the design load is less than 5%. The maximum error of the selected measurement points is less than 7%. The three calculation methods have high accuracy in the elastic range when calculating an SOSF with FCSK.

2. Under the maximum designed load, the structural displacement and strain are approximately linear. The maximum deflection in the test is 5.508 mm., which is span/908, indicating that the structure features good overall stiffness. During the entire test loading experiment, no macroscopic damage or cracks are observed, indicating the high safety margin of the structure.

3. Compared with the traditional STSK, the maximum Mises stress of the new type of shear key is reduced by 55.9%, the maximum deflection is reduced by 36.1%, and the bearing capacity is increased 2.56 times. The new type of shear key can significantly improve the load-bearing capacity and safety margin of the structure.

Author Contributions: Conceptualization, J Xiao and K Ma; Investigation, Q Wang, and W Zeng; Writing - original draft, R Shen; Writing - review & editing, J Xiao and R Shen; Funding acquisition, J Mao; Resources, G Li.

Editor: Marcílio Alves.

References

Bai, Y., Ma, K., (2018). Dynamic elasto-plastic analysis of new assembled multi-storey long-span honeycomb steel grid box structure. Paper Asia, COMPENDIUM 1 (4):28-33.

Bai, Z., Liu, X., Xing, D., Wei, Y., Ma, K., (2018). Experimental research on mechanics characteristics for shear block of steel tube with T-section steel ribs. Industrial Construction 48 (10):159-164.

Bakht, B., Jaeger, L.G., (1985). Bridge analysis simplified. McGraw-Hill: New York.

Chen, Z., Wu, G., Feng, D., Ma, K., (2018). Numerical study of the static and dynamic characteristics of reinforced concrete cassette structures for high-rise buildings. Struct Des Tall Spec, 28 (3).

Dong, S., Ma, K., Yan, H., Miao, C., (1992). Combination hollow rack. Hangzhou: Zhejiang University Press.

Huang, Y., Chen, B., Kang, Y., (1997). A new framing system – the open-web sandwich plate and the method of continuous analysis. Journal of Guizhou University of Technology 26 (04):66-72.

Huang, Y., Huang, J., Ma, K., (1998). Analysis of Vierendeel-sandwich-plate structure by the finite strip method. Journal of Guizhou University of Technology 27 (05): 97-101.

Jiang, L., Ma, K.J., Zhang, H., Wu, Q., Lu, H., Yang, Q., (2019). Seismic Behavior of Shear Connectors of Steel Vierendeel Sandwich Plate. Math Probl Eng (8047393).

Křístek, V., (1979). Theory of box girders. Wiley: Chichester, New York.

Liu, Z., Ma, K., Xiao, J., Sun, J., Liu, C., Zhao, Y., (2017). Effects of stiffened plate on static behavior of shear connector joints in steel open-web sandwich plate. Progress in Steel Building Structures 19 (02):29-37.

Luan, H., Ma, K., Qin, Y., Chen, Z., Wei, Y., (2017). Investigation of the structural behavior of an innovative steel open-web floor system. Int J Steel Struct 17 (4):1365-1378.

Luan, H.; Ma, K.; Qin, Y.; Li, X.; Chen, Z., (2016). Investigation on structural behavior of an innovative orthogonal-diagonal steel open-web sandwich floor system. Adv Struct Eng, 19(2):353-371.

Ma, K., Zhang, H., Zheng, T, (2006). Theory anda practice of new type architectural space gridding structures. Beijing: China Communications Press.

Makowski., Z.S., (1981). Analysis, design, and construction of double-layer grids. Applied Science Publishers, Halsted Press Division Wiley: London: New York.

Naderian, H., Sanches, R., Mercan, O., Kushner, P.J., Azhari, M., Ronagh, H., (2019). Stability of stiffened cruciform steel columns under shear and compression by the complex finite strip method. Thin Wall Struct 136: 221-234.

Nasrabadi, M.M., Torabian, S., Mirghaderi, S.R., (2013). Panel zone modelling of Flanged Cruciform Columns: An analytical and numerical approach. Engineering structures 49:491-507.

Reissner, E., (1947). On bending of elastic plates. Quart.appl.math. 5, 55-68.

Shang, H., Ma, K., Wei, Y., Lu, Y., (2019). Experimental Studies on Shear Resistance Performances for the Shear key of H Shape Steel Spatial Grid Roofs. Latin American Journal of Solids and Structures, 16 (UNSP e1895).

Shen, R., Xiao, J., Su, T., Mao, J., (2019). Steel-Concrete composite Open-web Sandwich Floor with Specially Shaped Shear Key. Chinese patent. ZL201920069745.1.

Wei, Y., Ma, K., Zhang, H., (2008). Analysis if static test for assembled monolithic steel Vierendeel sandwich plate. Journal of Guizhou University of Technology (Natural Science Edition) 37 (04):79-82.

Xiao, J., Ma, K., Dong, S., (2000). Equivalent shear strength formula for open-web lattice grid and open-web sandwich plate. Building Structure 30(4):39-54.

Xu, X.; Ma, K.; Liu, J.; Yuan, B.; Wei, Y., (2016). Experimental research on seismic behavior of steel grid frame wall. Earthquake engineering and engineering dynamics 36 (05):183-190.

Yang, Q., Ma, K., Hu, L., Zhang, H., Tan, Z., Wei, Y., (2013). Experimental study on load-carrying behavior of long-span assembled monolithic steel-concrete composite open-web plate. Journal of Building Structures, 34(10):32-40.